Model-based demand-limiting control of building thermal mass

Kyoung-ho Lee[a], James E. Braun[b],*

[a]*Korea Electric Power Research Institute, Korea Electric Power Corporation, Korea*
[b]*School of Mechanical Engineering, Purdue University, 140 S. Intramural Drive, West Lafayette, IN 47907 2031, USA*

Abstract

This paper describes the development and evaluation of a model-based approach for minimizing peak cooling demand using energy storage inherent in building structures. On any day where the strategy is invoked, the building is precooled with zone temperature setpoints at the low end of comfort prior to a demand-limiting (DL) period. The zone temperatures are then adjusted upwards during the demand-limiting period following a trajectory that keeps the peak cooling load below a specified target. The cooling demand target and setpoint trajectory are determined using a building model that is trained using field data. The overall approach was demonstrated for a building representative of a small commercial facility. The first step involved training the inverse model using a few weeks of hourly data. The model was then used to study the potential for peak load reduction and to determine setpoint trajectories that were implemented at the site. The demand-limiting strategy resulted in approximately 30% reductions in peak cooling loads compared to night setup control for a 5-h on-peak period of 1 PM to 6 PM.
© 2007 Elsevier Ltd. All rights reserved.

1. Introduction

It is generally necessary to consider the effect of thermal storage in building structures to estimate cooling requirements for sizing equipment. In particular, concrete floors, walls, and roofs used in commercial buildings dampen the effects of heat gains to the structure on the resulting gains to the interior air, leading to reduced peak cooling loads compared to less massive structures [1]. It is possible to obtain additional reductions in peak cooling through adjustments in zone temperature setpoints within bounds of thermal comfort.

Fig. 1 qualitatively compares zone temperature setpoint and cooling load variations for three different control strategies: conventional night-setup (NS) control, load-shifting control, and demand-limiting (DL) control. With NS control, the setpoint temperature is typically maintained in the middle of the comfort range during occupied periods and set up to a high setpoint during unoccupied periods. This strategy tends to minimize the total integrated cooling load and is the most common strategy for commercial buildings. Load-shifting control uses precooling (PC) with a setpoint temperature near the lower end of the comfort range prior to the occupied, on-peak period and then resets the setpoint to a fixed setpoint near the higher end of comfort during the on-peak period. As a result of the cooled thermal mass, less heat gain occurs to the air during the hours following the rise in setpoint than occurs for NS control. As the temperature of the building thermal mass increases, the effect of heat absorption decreases resulting in an increase in cooling load. This control strategy maximizes use of stored energy in the building mass and is appropriate for minimizing on-peak period electrical energy charges. With demand-limiting control, the building is precooled prior to an on-peak or critical peak-pricing period and then setpoints are adjusted in an optimal way so that the absorbed energy into the building thermal mass is controlled and the peak cooling load is minimized. This type of strategy is appropriate for minimizing on-peak demand charges or for use in a utility program where the utility takes active control for the end-user during periods of critical demand.

---

*Corresponding author.
 E-mail address: jbraun@purdue.edu (J.E. Braun).

Nomenclature

A	area (m^2 or ft^2)
$\mathbf{A}$	coefficient matrix in the state space representation
$\mathbf{B}$	coefficient matrix in the state space representation
C	capacitance (J/K or Btu/°F)
$\mathbf{C}$	coefficient matrix in the state space representation
DL	demand limiting control strategy
$\mathbf{D}$	coefficient matrix in the state space representation
E_{rms}	RMS error (%)
E	scalar transfer function coefficients for past histories of heat flow
G	radiation flux (W/m^2 or $Btu/h\,ft^2$)
h	convective heat transfer coefficient ($W/m^2\,K$ or $Btu/h\,ft^2\,°F$)
k_t	thermal conductivity ($W/m\,K$ or $Btu/h\,ft\,°F$)
N	number
NS	night-setup control strategy
PC	precooling control strategy
PLR	peak load ratio
Q	rate of heat transfer (W or Btu/h)
Q_b	rate of instantaneous heat gain to the building air (W or Btu/h)
$Q_{c,k}$	calculated cooling load at time step k (W or Btu/h)
$Q_{m,k}$	measured cooling loads at time step k (W or Btu/h)
$Q_{m,max}$	maximum measured load during testing period (W or Btu/h)
R	thermal resistance (K/W or °F h/Btu)
S	series of row vectors containing transfer function coefficients for past histories of heat flow
T	temperature (°C or °F)
t	time (h)

$\mathbf{u}$	vector of input variables
$\mathbf{x}$	vector of state variables
$\mathbf{Y}$	vector of output variables

Greek

τ_{eff}	effective window transmittance for solar radiation
ρ	density (kg/m^3 or lb/ft^3)

Subscripts

a	ambient
avg	average
b	building
c	building cooling load
cool	cooling capacity
dl	DL control
e	external wall
eff	effective
f	floor or final
g	ground
g, rad	radiative internal heat gain
g, conv	convective internal heat gain
i	internal or initial
k	time stage
max	maximum
ns	night-setup control
occ	occupied period
op	on-peak period
r	roof and ceiling
sol	solar
test	test period
unocc	unoccupied period
w	window
x	state variable
z	zone
zo	adjacent zone

As noted by Braun [2], there are four opportunities for reducing operating costs associated with load-shifting and demand-limiting strategies: (1) use of low temperature nighttime air for ventilation precooling, (2) improved mechanical cooling system efficiency due to more favorable operation at lower ambient and part-load conditions, (3) reduction in on-peak electrical energy charges, and (4) reductions in on-peak electrical demand charges. The first two opportunities lead to reduced building energy usage, whereas the second two incentives change the time variation in electrical energy requirements but can result in increased overall usage due to lower average zone temperature setpoints. However, an increase in electrical energy usage at the building can actually result in a reduction in primary energy usage at the power plant if the electrical energy is used at times of lower power plant capacity when more efficient

equipment is employed. This is one of the reasons that electric utilities provide rates that encourage users to reduce electrical usage and peak demand during on-peak periods. The current paper addresses control strategies for achieving demand-limiting control and not load-shifting control.

There have been a number of studies that have considered the impact of zone temperature setpoint adjustments on load shifting and peak load reduction, including studies by Braun [2], Ruud et al. [3], Rabl and Norford [4], Reddy et al. [5], Keeney and Braun [6,7], Braun et al. [8], and Xu et al. [9,10]. In particular, these studies demonstrated very significant potential for peak demand reduction when setpoints were adjusted in an optimal manner. However, these papers did not present general approaches for determining setpoint trajectories that minimize peak electrical power or cooling load.
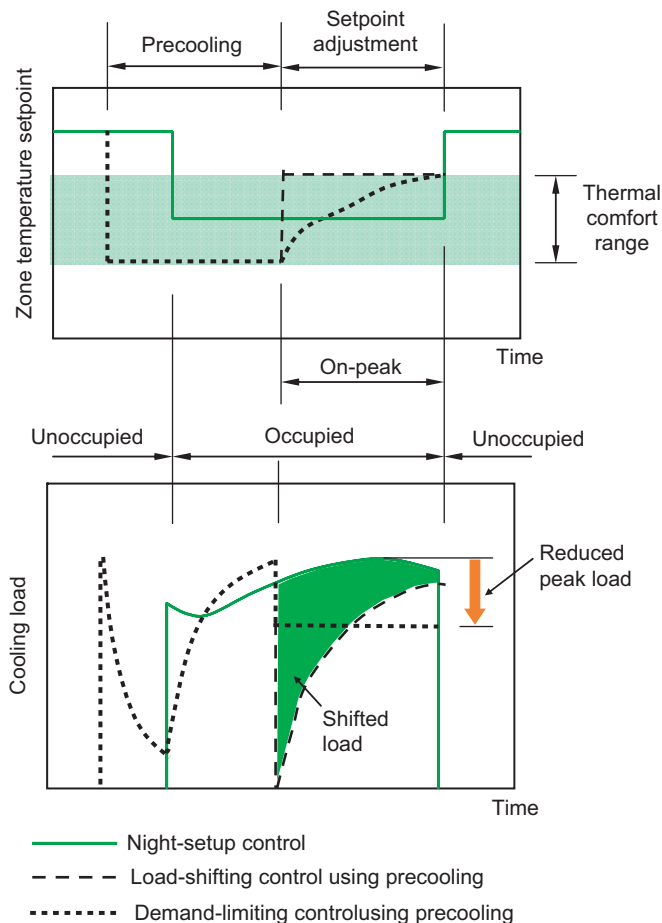
Fig. 1. Comparison of night setup, load shifting, and demand-limiting control.

The current paper describes development of a model-based demand-limiting control strategy that utilizes an inverse building model presented by Chaturvedi and Braun [11]. The use of an inverse model trained with field data allows determination of setpoint trajectories that are near-optimal for a specific building. The overall approach was demonstrated and evaluated for a building representative of a small commercial facility. The inverse model was trained using hourly data from a previous study. The model was then used to study the potential for peak load reduction and to determine setpoint trajectories that were implemented at the site. Measured cooling loads for demand-limiting control were compared with those for night setup control to evaluate peak load reduction. In addition, an occupant comfort survey was performed. Details of the experiments and results were previously presented by Lee and Braun [12], whereas the current paper focuses on the method development and performance evaluation.

2. Description of test building

2.1. Description of building

The facility used in this study is the Energy Resource Station (ERS) building that houses the Iowa Energy Center

(see [13] for a detailed description). The building includes a set of unoccupied test rooms that are well instrumented for comparative testing as well as occupied areas for building employees. Fig. 2 shows a schematic floor plan of the ERS building that identifies the test rooms and occupied areas. The eight test rooms are organized in identical pairs (labeled "A" and "B") with three sets of zones having one exterior wall (east, west, and south) and one set that is internal. Collectively, the four pairs of zones are representative of a small commercial building. Each test room has $25.55\,m^2$ $(274.97\,ft^2)$ of floor area and the ceiling is $2.59\,m$ $(8.5\,ft)$ high. The height of plenum zones above the test zones is $1.68\,m$ $(5.5\,ft)$. The exterior zones have $6.87\,m^2$ $(74\,ft^2)$ of window area. No blinds were used. In this study, the test zones were used for evaluating peak load reductions for demand-limiting, whereas the occupied areas were used for evaluating occupant comfort. The occupied areas are composed of office space, a display room, a computer center, two classrooms, service rooms, a media center, a reception space, and a mechanical room. The locations of subjects in the occupied areas who participated in the comfort survey are depicted in Fig. 2.

Lee and Braun [12] give detailed information regarding construction materials and internal gains for the test rooms within the ERS building. The exterior walls, floor, and roof are relatively heavyweight. However, most of the thermal mass is not well connected in a thermal sense to the interior air. The exterior walls have $10.16\,cm$ $(4\,in)$ pre-cast concrete panels on the outside but are separated from the internal space by an air gap, insulation, and gypsum. The roof utilizes $20.32\,cm$ $(8\,in)$ pre-cast cored concrete panels but is separated from the internal space by a return and acoustic tiles. The floors are carpeted. Furthermore, there is no additional internal mass within the test rooms in the form of internal walls or furnishings that would normally be found in commercial buildings. In addition to lighting internal gains, internal gains due to equipment
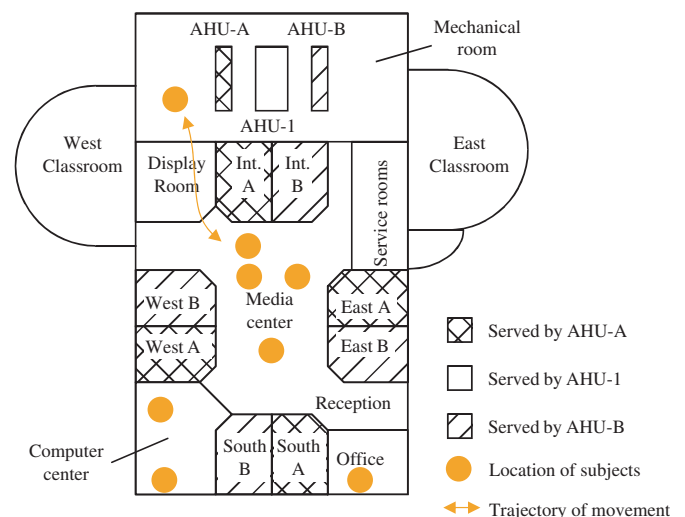

Fig. 2. Schematic diagram of floor plan for ERS building.

(e.g., computers) and people were simulated using baseboard electric heaters. There were no occupants present within the test rooms during testing. The combination of test rooms is thought be representative of a small commercial building in terms of size, surface area-to-volume ratio, internal gains, and coupling between the thermal mass and zone air.

Braun et al. [14] used the ERS building to demonstrate the potential for load shifting associated with a simple building thermal mass precooling strategy. The test was performed for 17 days in August of 2001. These data were used for training the inverse model for the current paper.

2.2. Data measurement

Weather data were provided by a weather station located at the ERS [13], including outdoor air dry-bulb temperature and relative humidity, wind speed and direction, atmospheric pressure, total normal incidence solar flux, and global horizontal solar flux. Table 1 shows sensor accuracy for measurements from the weather station.

Test room data included room air temperature and supply air temperature and flow rate, whose accuracies are listed in Table 2. Test room cooling loads were calculated using these three measurements. The supply air temperature was measured using an array of 4 platinum 1000Ω RTD probes. An air temperature RTD probe was located on a stand near the center of each test room to measure room air temperatures. The air flow rate was determined from a velocity pressure difference measured using a flow ring and differential pressure sensor at the inlet to the VAV box. All data used in this study were averaged over an hourly interval.

Table 1
ERS weather station measurement accuracy

Name	Accuracy
Outdoor air temperature	$\pm 0.1\,°C\ (\pm 0.18\,°F)$
Outdoor air humidity	$\pm 2\%$
Wind velocity	$\pm 0.45\,m/s\ (\pm 1\,mph)$
Wind direction	$\pm 1°$
Normal incidence solar flux	$\pm 0.5\%$ reading
Global horizontal solar flux	$\pm 0.5\%$ reading
Atmospheric pressure	$\pm 0.75\,mbar$

Table 2
Test room measurement accuracy

Name	Accuracy
Room temperature	$\pm 0.14\,°C\ (\pm 0.25\,°F)$
Room supply air temperature	$\pm 0.14\,°C\ (\pm 0.25\,°F)$
Room supply air flow rate	$\pm 1.13\,m^3/min\ (\pm 40\,cfm)$ for east, south, and west rooms
	$\pm 0.71\,m^3/min\ (\pm 25\,cfm)$ for interior rooms

3. Dynamic inverse building model

3.1. Model development

Fig. 3 shows the thermal network employed for the inverse model of the ERS building that was developed from the model of Chaturvedi and Braun [11]. All test zones (west, east, south, and interior rooms) were modeled as a single zone using a single external wall, an internal wall, a roof and a floor. Predicted and measured cooling loads were for the combined test rooms at the ERS, which is representative of a small commercial building.

Each of the walls was represented with two capacitors and three resistors. It was assumed that solar radiation through windows was absorbed only on the floor. Since internal radiation is due to lights located on the ceiling, internal radiative gains were distributed only to the walls and floor. Infiltration and radiation between the building outside surface and night sky were not considered. The temperature in the adjacent occupied areas, T_{zo}, was assumed to be equal to the temperature within the test rooms at all times, T_z.

Using an energy balance at each node having a capacitor, a state-space formulation was set up for the building model as described by Chaturvedi and Braun [11]:

$$\frac{d\mathbf{x}_b}{dt} = \mathbf{A}_b \mathbf{x}_b + \mathbf{B}_b \mathbf{u}_b, \tag{1}$$

$$\mathbf{Y}_b = Q_b = \mathbf{C}_b \mathbf{x}_b + \mathbf{D}_b \mathbf{u}_b, \tag{2}$$

where Q_b is the rate of instantaneous heat gain to the building air, $\mathbf{A}_b$, $\mathbf{B}_b$, $\mathbf{C}_b$ and $\mathbf{D}_b$ are matrices and vectors of coefficients determined by the resistors and capacitors, and $\mathbf{x}_b$ and $\mathbf{u}_b$ are vectors of states and inputs given by

$$\mathbf{x}_b^T = [T_{r1}, T_{r2}, T_{e1}, T_{e2}, T_{f1}, T_{f2}, T_{i1}, T_{i2}], \tag{3}$$

$$\mathbf{u}_b^T = [T_z, T_a, T_g, Q_{sol,r}, Q_{sol,e}, Q_{g,rad,f}, Q_{g,rad,e}, Q_{g,rad,i},$$
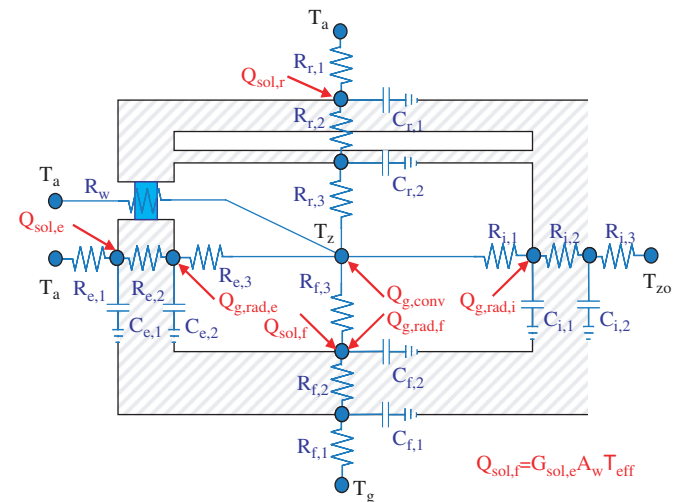$$\times Q_{sol,f}, Q_{g,conv}]. \tag{4}$$

Fig. 3. Thermal network for inverse building model.

The eight state variables arise from having two nodal temperatures in each of the four structural elements. The 10 input variables are zone temperature, ambient temperature, ground temperature, solar radiation absorbed on external walls and on the roof, internal radiative gains for the floor, external walls, and internal walls, solar radiation transmitted through windows that is absorbed on the floor, and internal convective gains to the interior air. The ground temperature was assumed constant and was estimated using experimental results from Thomas and Rees [15] and Zhou et al. [16] to be 17.5 °C (63.5 °F). Internal radiative gains were distributed assuming an equal heat flux to the interior surfaces of the walls and floor. Lighting was assumed to be 90% radiative and 10% convective, whereas the heaters used to simulate other internal gains were assumed to be 5% radiative and 95% convective.

The state-space formation given in Eqs. (1) and (2) only considers transients associated with the building structure and can be used to estimated the heat gain to the air for a specified zone temperature. A separate energy balance on the air is used to determine sensible zone cooling loads when considering zone temperature transients.

$$C_{z,eff} \frac{dT_z}{dt} = Q_b - Q_c, \qquad (5)$$

where $C_{z,eff}$ is an effective zone thermal capacitance involving the zone air and internal mass and Q_c is sensible cooling load.

The state-space representation is solved assuming a 1-h time interval using the methodology of Seem et al. [17] to obtain a comprehensive transfer function for heat gain in terms of the input variables and previous heat gains as

$$Q_{b,k} = \left(\sum_{j=0}^{N_x} \mathbf{S}_{b,j} \mathbf{u}_{b,k-j} \right) - \left(\sum_{j=1}^{N_x} \mathbf{e}_{b,j} Q_{b,k-j} \right), \qquad (6)$$

where the matrix $\mathbf{S}_{b,j}$ and vector $\mathbf{e}_{b,j}$ contain transfer function coefficients determined using $\mathbf{A}_b$, $\mathbf{B}_b$, $\mathbf{C}_b$, and $\mathbf{D}_b$, The subscript $k-j$ denotes the time interval associated with the inputs and net air heat gain. This time-series equation relates the current heat gain to current and previous inputs and previous heat gains. For application of Eq. (6), the inputs and heat gains are assumed to be constants over each time interval, evaluated using average values.

Eq. (6) provides an estimate for average heat gain over a given interval with a specified zone temperature setpoint. If different setpoints are employed for the start and end of the interval, the setpoint is assumed to vary linearly and the average zone temperature used in Eq. (6) is determined as

$$T_{z,k} = \frac{T_{z,k,i} + T_{z,k,f}}{2}, \qquad (7)$$

where the subscripts i and f denote initial and final values for interval k.

Eq. (5) is approximated according to

$$C_{z,eff} \frac{T_{z,k,i} - T_{z,k,f}}{\Delta t} = Q_{b,k} - Q_{c,k}, \qquad (8)$$

where Δt is the time step for the model

Eq. (8) is used along with Eqs. (6) and (7) to determine the average zone sensible cooling rate for a given interval for specified initial and final setpoint temperatures. If the required cooling rate is negative, then there is no cooling requirement and the zone temperature should "float" during this interval. For this case, the zone sensible cooling load $Q_{c,k}$ is set to zero and Eqs. (6)–(8) are resolved for the floating final and average zone temperatures over the interval, $T_{z,k,f}$ and $T_{z,k}$.

3.2. Model training

The training algorithm is divided into two phases, a global search and a local search as described by Chaturvedi and Braun [11]. The global search uses a systematic search to determine reasonable values of the building resistors and capacitors within bounds determined from a crude building description. The local search uses a local non-linear regression method to further improve the R and C estimates by minimizing the root-mean-squared error between measured and calculated cooling loads for the training duration. The combination of a local and a global phase provides a robust algorithm for determining an accurate model and only requires minimal preliminary building information. Parameters determined through global and local searches are: effective window transmittance for solar radiation, effective zone capacitance, and the thermal resistances and capacitances shown in Fig. 2. Effective zone capacitance appears in Eq. (8) and effective transmittance is used to calculate solar gains through windows.

Tables 3 and 4 give the bounds used for the global search in the model training for the ERS building. Thermal conductivities (k_t) for the walls, and convective heat transfer coefficients (h_i and h_e) for the building inside and outside wall surfaces are used in determining thermal resistances for each wall element in the thermal network model depicted in Fig. 3. Densities and specific heats of each wall element are used to determine thermal capacitances for each wall element. Additionally, information on building wall thickness and surface area is necessary. The effective solar transmittance τ_{eff} is used to determine solar transmission through the windows.

Measured data obtained in the summer of 2001 at the ERS and presented by Braun et al. [14] were used to initially train and test the model. The testing consisted of a period with night setup control (9 days from August 3 to 11, 2001) and a period with precooling and load-shifting control (8 days from August 13 to 20, 2001). A part of the data was used for model training, and the remainder was used for testing. Table 5 represents four cases that were considered for training and testing of the inverse model.

Table 3
Material property bounds used in model training algorithm

Property	Bounds	Element type			
		External wall	Internal wall	Roof and ceiling	Floor
k_t [W/K m (Btu/h F ft)]	Min	1.7E-3 (1E-3)	1.7E-3 (1E-3)	1.7E-5 (1E-5)	1.7E-3 (1E-3)
	Max	1.7 (1.0)	1.7 (1.0)	8654 (5E3)	1.7 (1.0)
$\rho*C_p$ [kJ/K m^2 (Btu/F ft^3)]	Min	6.7 (0.1)	6.7 (0.1)	6.7 (0.1)	6.7 (0.1)
	Max	2012 (30)	670.7 (10)	3353 (50)	2012 (30)

Table 4
Physical property bounds used in model training algorithm

Bounds	τ_{eff}	h_i [W/m^2 K (Btu/h ft^2 °F)]	h_e [(W/m^2 K (Btu/h ft^2 °F)]	$C_{z,eff}$ [kJ/K (Btu/°F)]
Min	0.1	0.57 (0.1)	11.4 (2.0)	0 (0)
Max	0.9	5.7 (1.0)	34.1 (6.0)	1519 (800)

Table 5
Data sets for different training and testing cases

Data set cases	Training	Testing
I	Night setup (9 days)	Load shifting (8 days)
II	Load shifting (8 days)	Night setup (9 days)
III	First 6 days of night setup + load shifting (14 days)	Repetition of last 3 days of night setup (9 days)
IV	Night setup + first 5 days of load shifting (14 days)	Repetition of last 3 days of load shifting (9 days)

Fig. 4. E_{rms} of inverse model with four cases of training and testing data sets.

In cases III and IV, portions of data from both night setup and precooling tests were used for training. In each of these cases, only three days of data were not used for training and these three days were repeated three times in sequence to obtain 9-day test sequences.

Model performance is described in terms of a prediction error defined as

$$E_{rms}(\%) = \frac{100}{Q_{m,max}} \sqrt{\sum_{k=1}^{N_{test}} (Q_{m,k} - Q_{c,k})^2 \Big/ (N_{test} - 1)}, \quad (9)$$

where $Q_{m,k}$ is measured cooling load at hour k, $Q_{c,k}$ is the cooling load calculated with the inverse building model, and $Q_{m,max}$ is the maximum measured cooling load for the test data.

3.3. Model validation

Fig. 4 shows performance of the inverse model under test conditions for the different cases outlined in Table 5. Generally the model provides reasonably good predictions of hourly cooling loads compared with measurements. However, the model accuracy is sensitive to the data set used for training. It is best to have training data for days operating with different control strategies for adjusti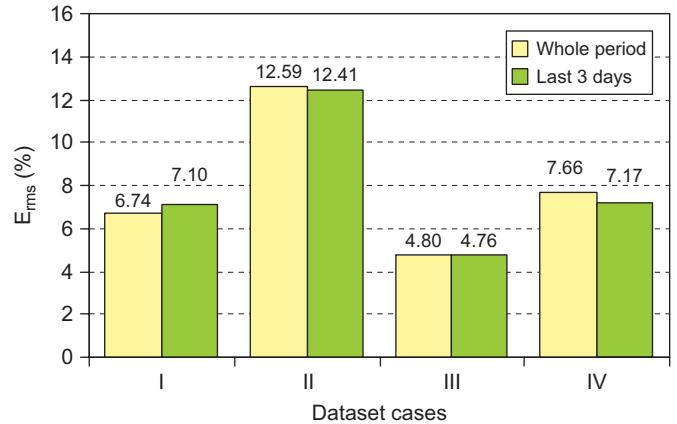ng zone temperature setpoints. A better model could be obtained if more data were available at a wider range of conditions.

Fig. 5 compares calculated and measured cooling loads for two-day sequences from the test periods for night setup and load-shifting control. All of the available data were used for training the model. The two-day sequences had similar ambient temperature and solar radiation conditions. Therefore, the cooling loads shown in Fig. 5 are useful for evaluating the impact of precooling on load shifting as well as evaluating model performance. The model very accurately predicts the load shifting and peak load reduction associated with the load-shifting control strategy. For both simulated and measured results, the occupied period load was about 23% less for the precooling tests and the peak load was reduced by about 9%.

Training results from the model parameter estimation process are presented in Table A.1 in Appendix. The sum of all the estimated thermal capacitances for the building is 197.3 MJ/K (103,869 Btu/°F). In order to assess the relative magnitude of this capacitance, it is useful to compare it to
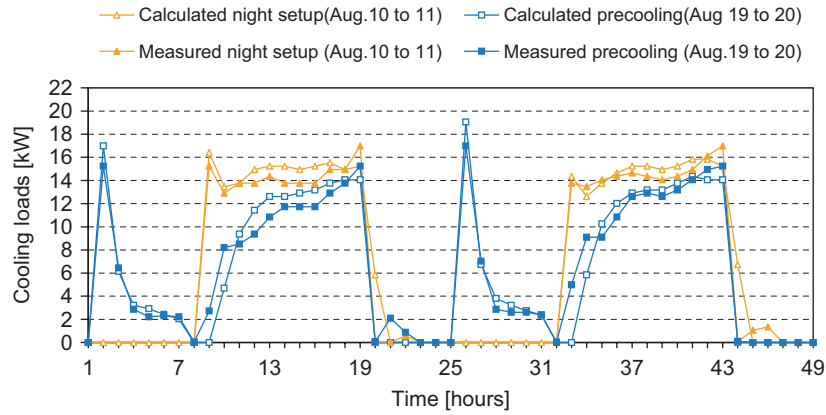
Fig. 5. Comparison of measured and simulated cooling loads (inverse model) for night setup and precooling control strategies.

a typical daily cooling load of 580.4 MJ (550,071 Btu) that occurred on the August 11 test day for night setup control. If all of the thermal capacitance could be precooled by about 3 °C (5.4 °F), then practically all of the daytime cooling load could be shifted to nighttime hours. However, only mass that is physically close to the internal zone air is effective. For comparison, the capacitance associated with the internal mass node described in Eq. (5) was estimated to be about 6% of the total capacitance or 11.4 MJ/K (5993.48 Btu/°F). However, energy storage for demand limiting occurs in the internal zone node and wall, floor and ceiling nodes closest to the zone air. The effective thermal capacitance would probably be somewhere between the internal and total building capacitance values, but closer to the internal capacitance.

4. Model-based demand-limiting control methodology

The load-shifting strategy used to obtain the results of Fig. 5 was not designed to maximize peak load reduction. Much greater peak load reduction is possible if the zone temperatures were varied within the comfort region rather than being held constant. Such a strategy would keep the zone temperatures low at the beginning of occupancy and raise them later in the day. This would have the effect of increasing the early occupancy loads and decreasing the late occupancy loads. This section presents a method for determining zone temperature setpoints that minimize peak cooling demand during a specified demand-limiting period.

A demand-limiting control strategy in this work is defined as a strategy that aims to "limit" the peak cooling load under a specified target cooling load during a demand-limiting period by adjusting room setpoint temperature within the comfort range. Fig. 6 represents setpoint temperatures for both NS and demand-limiting control strategies where t is time and T is temperature and the subscripts "occ" and "unocc" denote unoccupied and occupied period, "NS" and "demand-limiting" mean night setup and demand-limiting strategies, "max" indicates the upper limit of thermal comfort, i refers to start of a period, and f means end of a period.
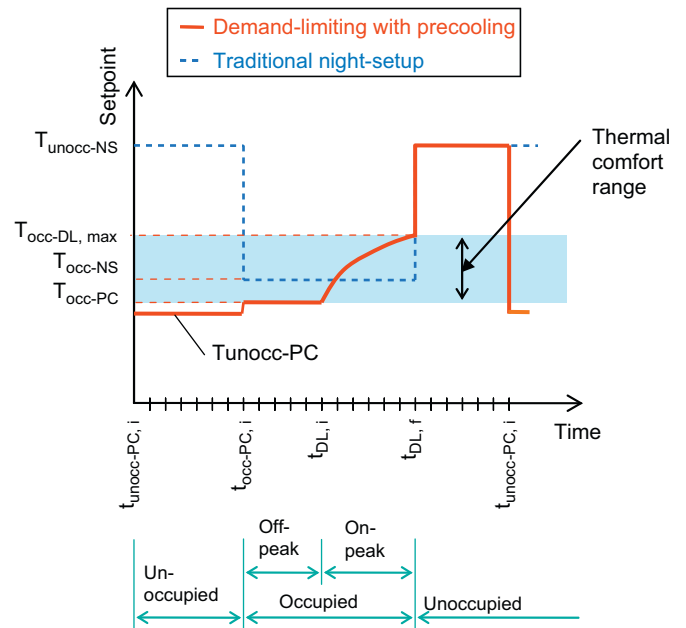

Fig. 6. Setpoint temperatures for night setup and demand-limiting strategies.

The term "Model-Based, demand-limiting Control" in this study means that a numerical algorithm is used along with an inverse model to determine an optimal setpoint trajectory that minimizes peak cooling demand during a demand-limiting period. The optimization problem for determining a setpoint trajectory that minimizes the maximum (peak) cooling hourly (or sub-hourly) load during the demand-limiting period involves minimization of the following cost function

$$J = \max\{Q_{c,k}(T_{z,k})\} \quad k = 1, \ldots, k_{DL} \tag{10}$$

with respect to $T_{z,k}$ subject to $T_{occ-PC} \leqslant T_{z,k} \leqslant T_{occ-DL,max}$ and $0 \leqslant Q_{c,k} \leqslant Q_{cool,max}$ where $Q_{cool,max}$ is capacity of the cooling equipment and k_{DL} is the final time stage during the demand-limiting period. It was determined through numerical optimization that the solution to this minimization problem results in a constant cooling rate during times

when the optimal setpoints are between the minimum and maximum allowable setpoints and lower cooling rates when the setpoints are constrained to the minimum or maximum temperature constraints. With this knowledge, the optimization problem is replaced with a numerical scheme that determines the constant cooling rate that keeps zone temperatures between the bounds.

A Secant method is used to find the target cooling rate that satisfies the following residual function

$$f(Q_{c,target}) = T_{z,k_{DL}} - T_{occ-DL,max} = 0, \qquad (11)$$

subject to the following constraints for k between 1 and k_{DL}:

$$T_{occ-PC} \leqslant T_{z,k} \leqslant T_{occ-DL,max}, \qquad (12)$$

$$Q_{c,k} = \min(Q_{c,target}, Q_{max,k}), \quad k = 1, \ldots, k_{DL}, \qquad (13)$$

where $T_{z,k_{DL}}$ is zone temperature at the end of on-peak period, T_{occ-PC} is zone temperature zone temperature at the end of the occupied precooling period, $T_{occ-DL,max}$ is upper bound zone temperature during the on-peak period, $Q_{max,k}$ is maximum cooling rate that can be applied for hour k, $Q_{c,target}$ is target load for demand-limiting during the on-peak period, and $Q_{c,k}$ is the applied building cooling rate for hour k. For each iteration of the Secant method, the building is precooled at a constant setpoint $T_{unocc-PC}$ for a specified duration. During the on-peak period, the setpoint is set at the lower end of the comfort limit at T_{occ-PC} (e.g., 20.6 °C (69 °F)) until the cooling load exceeds the target demand-limiting cooling load. When the building cooling load exceeds the target load, the setpoint temperature increases in order to limit the building cooling load to the target load. The iteration process adjusts the target load so as to utilize the entire comfort range where the zone temperature at the end of occupied period is at the upper end of comfort $T_{occ-DL,max}$ (e.g., 24.4 °C (76 °F)). After the occupied period, the setpoints are set up to $T_{unocc-NS}$ (e.g., 26.7 °C (80 °F)) until the start of the precooling period.

5. Identifying an appropriate demand-limiting control strategy

5.1. Approach

The trained model was used along with the demand-limiting algorithm in order to investigate the impact of different control variables on demand reduction and determine an appropriate strategy to test at the ERS building. The last day of night setup testing from 2001 (August 11) was chosen for comparison with a base case of night setup control. Every simulation was conducted for an identical set of 10 days in a row to erase the effects of initial conditions and reach a steady-periodic condition. Cooling loads occurred during occupancy from 7 AM to 6 PM.

Table 6 shows the range of parameters considered in this study where the parameters are defined in Fig. 6. The

Table 6
Parameters used in simulation study

Parameters	Description	Values
$t_{unocc-PC,i}$	Initial time of precooling during unoccupied period	{10PM, 12AM, 2AM, 4AM, 6AM}
$t_{occ-PC,i}$	Initial time of precooling during occupied period	{7AM}
$t_{DL,i}$	Initial time of demand-limiting period	{7AM, 9AM, 11AM, 1PM, 3PM}
$t_{DL,f}$	Final time of demand-limiting period	{6PM}
T_{occ-PC}	Precooling setpoint temperature during occupied period	{19.4, 20.6, 21.7, 22.8 °C} ({67, 69, 71, 73 °F})
$T_{unocc-PC}$	Precooling setpoint temperature during unoccupied period	{17.2, 18.3, 19.4, 20.6 °C} ({63, 65, 67, 69 °F})
$T_{occ-DL,max}$	Maximum setpoint temperature during demand-limiting period	{23.3, 24.4, 25.6, 26.7 °C} ({74, 76, 78, 80 °F})
T_{occ-NS}	Setpoint temperature during occupied period under night-setup control	{22.2, 23.3, 24.4, 25.6, 26.7 °C} ({72, 74, 76, 78, 80 °F})
$T_{unocc-NS}$	Setpoint temperature during unoccupied period under night-setup control	{26.7 °C} ({80 °F})

demand-limiting period, or on-peak period where the demand-limiting strategy is applied, was varied by changing the start-time (DL start time) from 7 AM to 3 PM for a fixed end time of 6 PM. The precooling period was also changed by varying the start-time ($t_{unocc-PC,i}$) from 10 PM to 7 AM. A start-time of 7 AM for precooling represents no unoccupied period precooling and is a limiting case.

The performance of the demand-limiting strategy was measured in terms of a peak load ratio (PLR) defined as the ratio of the peak load under the demand-limiting strategy to the peak load for the base case NS strategy or

$$PLR = \frac{\max\{Q_{c,k,DL}\}}{\max\{Q_{c,k,NS}\}_{@T_{occ-NS}=23.3\ C°(74\ °F)}},$$
$$\text{for} \quad k = t_{DL,i}, \ldots, t_{DL,f}. \qquad (14)$$

The base case NS strategy had an unoccupied setpoint at $T_{unocc-NS}$ of 26.7 °C (80 °F) and an occupied setpoint at T_{occ-NS} of 23.3 °C (74 °F).

For NS control, the impact of the occupied setpoint on demand was also considered. In this case, a PLR under NS (PLR$_{NS}$) is defined as

$$PLR_{NS} = \frac{\max\{Q_{c,k,NS}\}_{@T_{occ-NS}}}{\max\{Q_{c,k,NS}\}_{@T_{occ-NS}=23.3\ °C(74\ °F)}},$$
$$\text{for} \quad k = t_{DL,i}, \ldots, t_{DL,f}. \qquad (15)$$

5.2. Simulation results

The effects of start times for demand limiting and night precooling on peak cooling load reduction are shown in Fig. 7. The temperature setpoints for these results are $T_{unocc-PC} = 19.4\,°C$ (67 °F), $T_{occ-PC} = 20.6\,°C$ (69 °F), $T_{occ-DL,max} = 24.4\,°C$ (76 °F), and $T_{unocc-NS} = 26.7\,°C$ (80 °F). PLR has a small dependence on the precooling duration ($t_{unocc-PC,i}$) when the demand-limiting period begins in the afternoon. However, precooling becomes more important as the start of the demand-limiting period moves earlier in the day. For a demand-limiting period beginning at 7 AM, the maximum peak load reduction was about 23% compared to NS control. For an afternoon start to the on-peak period, the peak load reduction for the on-peak period was about 40% even without any precooling.

Figs. 8 and 9 show selected detailed results from the cases considered for Fig. 7. These figures compare hourly cooling loads and zone temperatures for the NS and demand-limiting strategies for a morning and afternoon start to the demand-limiting period. For the results of Fig. 8, the demand-limiting strategy involved precooling the building from midnight to 7 AM and demand-limiting began at 7 AM. The peak load under NS occurred around 5 PM in the afternoon. As a result of precooling, the demand-limiting strategy resulted in very low loads during the early morning hours. When the load reached the target,
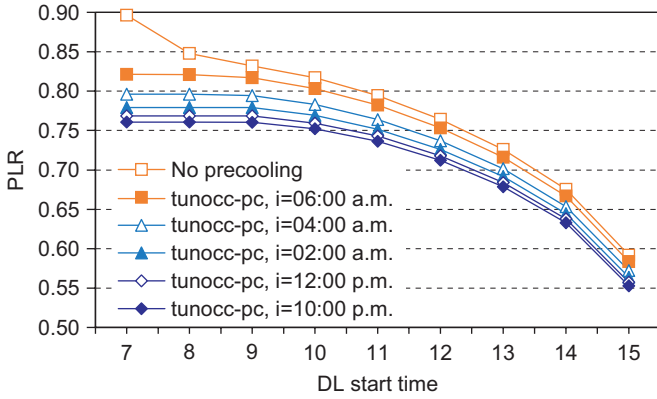

Fig. 7. PLR with $t_{unocc-PC,i}$ varying demand-limiting start time.
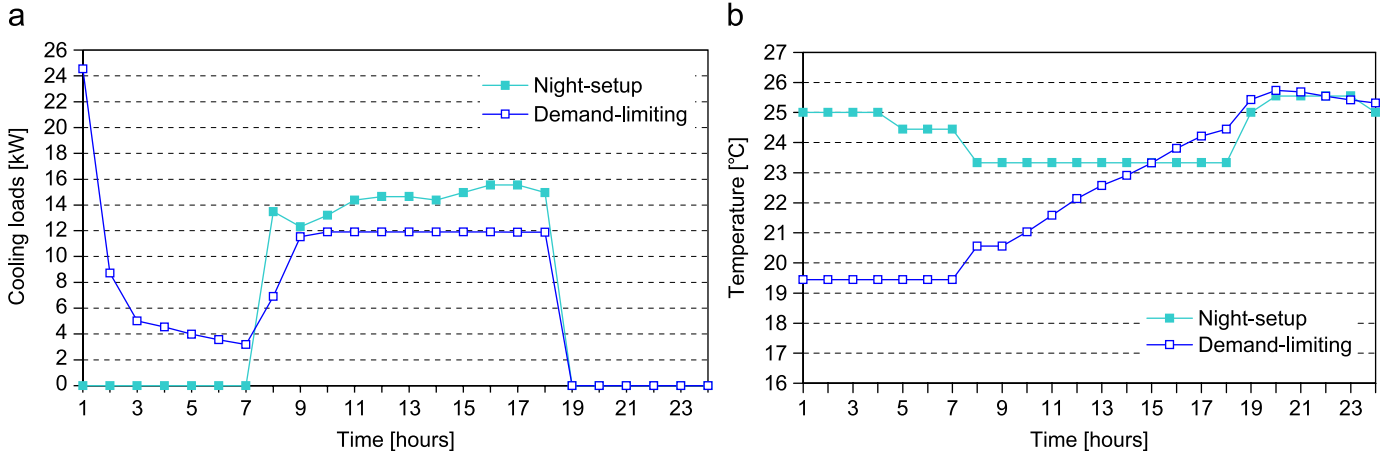

Fig. 8. Simulated NS and demand-limiting control (precooling start-time ($t_{unocc-PC,i}$) of midnight and demand-limiting start-time of 7 AM): (a) cooling load and (b) zone temperature.
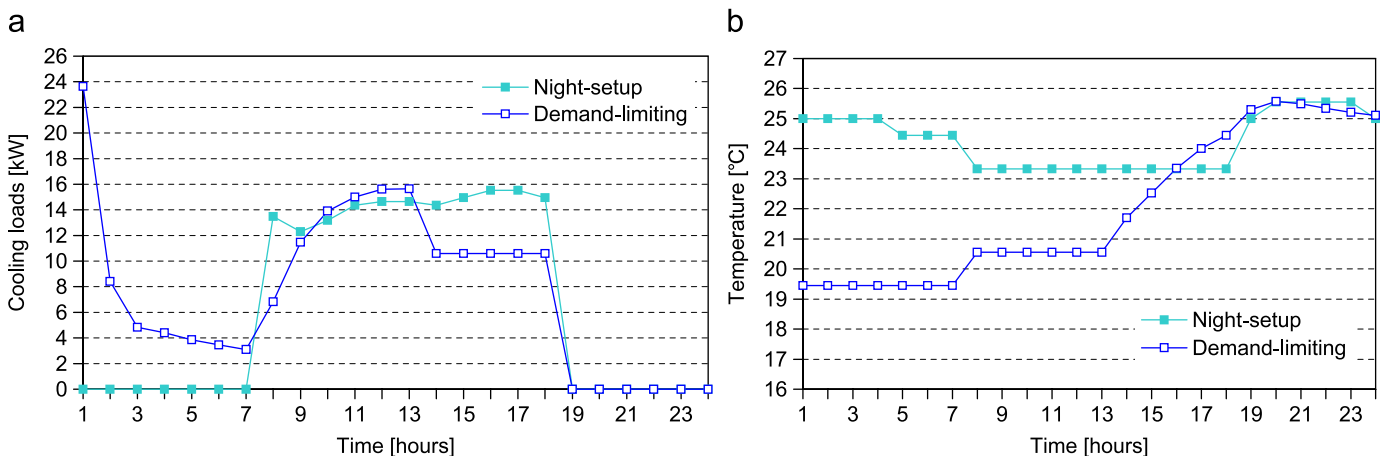

Fig. 9. Simulated NS and demand-limiting control (precooling start-time ($t_{unocc-PC,i}$) of midnight and demand-limiting start-time of 1 PM): (a) cooling load and (b) zone temperature.

then the setpoint was raised following a trajectory that kept the load constant. The zone temperature setpoint increased until it reached 24.4 °C (76 °F) at the end of the demand-limiting period. For the results of Fig. 9, the start time for demand limiting was 1 PM. As a result, the setpoint was kept low during the morning hours for the demand-limiting strategy and the late morning loads were slightly greater than those for the NS control. With a short demand-limiting period, the peak reduction was significantly greater than for the results of Fig. 8. The energy storage is more significant compared to the total load for a shorter demand-limiting period. Although not shown here, the application of demand-limiting control without precooling results in a significant early morning load spike that occurs at the start of the occupied period.

Fig. 10 shows how PLR is affected by the variation of $T_{\text{occ–PC}}$ (setpoint temperature during the off-peak occupied period) under demand-limiting control. Other setpoint conditions were $T_{\text{unocc–NS}} = 26.7\,^\circ\text{C}$ (80 °F), $T_{\text{unocc–PC}} = 19.4\,^\circ\text{C}$ (67 °F), $T_{\text{occ–PC}} = 24.4\,^\circ\text{C}$ (76 °F), and $t_{\text{unocc–PC},i} = 12$ midnight. Peak load reduction increases (PLR decreases) with decreasing $T_{\text{occ–PC}}$, with a greater impact occurring for shorter demand-limiting periods. The effect of demand-
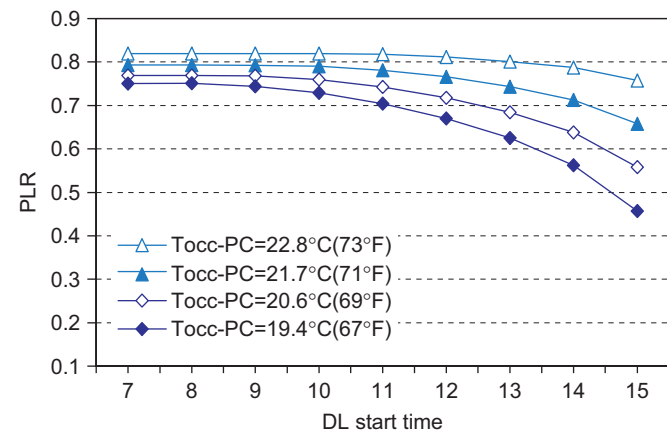

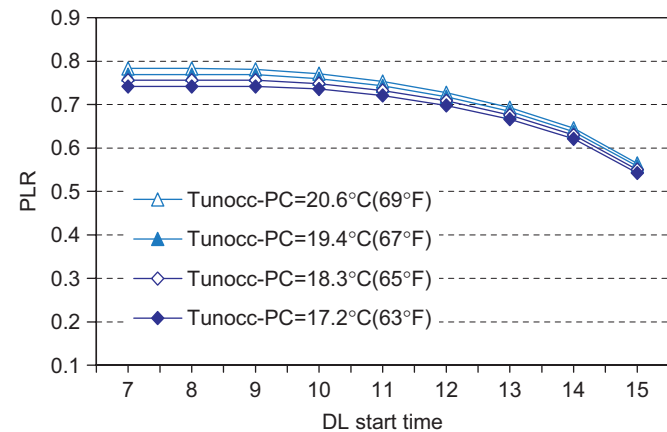Fig. 10. PLR with on $T_{\text{occ–PC}}$ and demand-limiting start time.

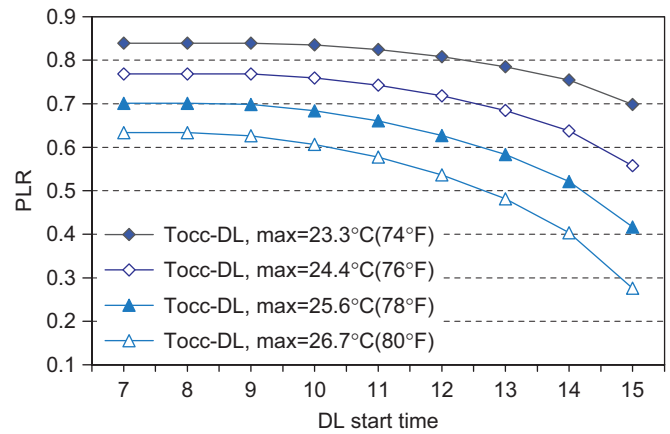Fig. 11. PLR with $T_{\text{unocc–PC}}$ varying demand-limiting start time.

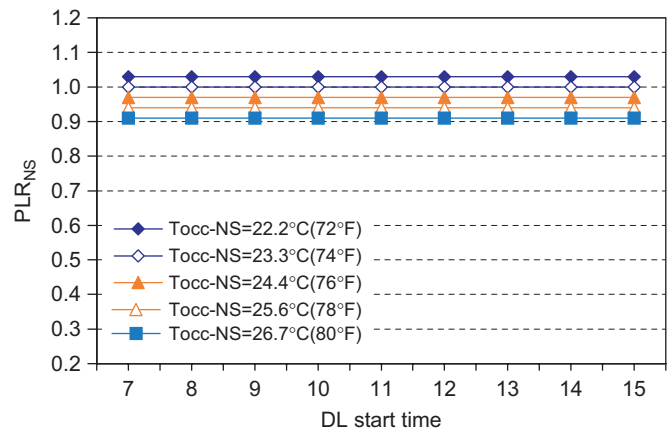Fig. 12. PLR with $T_{\text{occ–DL,max}}$ varying demand-limiting start time.

Fig. 13. PLR$_{\text{NS}}$ with $T_{\text{occ–NS}}$ varying demand-limiting start time.

limiting start-time on peak load reduction becomes greater as $T_{\text{occ–PC}}$ is reduced.

Fig. 11 shows the impact of $T_{\text{unocc–PC}}$ (setpoint for night-precooling during the unoccupied period) on PLR. Other setpoint conditions were $T_{\text{unocc–NS}} = 26.7\,^\circ\text{C}$ (80 °F), $T_{\text{occ–PC}} = 20.6\,^\circ\text{C}$ (69 °F), $T_{\text{occ–DL,max}} = 24.4\,^\circ\text{C}$ (76 °F), and $t_{\text{unocc–PC},i} = 12$ midnight. The impact of $T_{\text{unocc–PC}}$ is small and PLR decreases slightly as $T_{\text{unocc–PC}}$ is lowered.

Fig. 12 shows PLR as a function of $T_{\text{occ–DL,max}}$. Other setpoint conditions were $T_{\text{unocc–NS}} = 26.7\,^\circ\text{C}$ (80 °F), $T_{\text{unocc–PC}} = 19.4\,^\circ\text{C}$ (67 °F), $T_{\text{occ–PC}} = 20.6\,^\circ\text{C}$ (69 °F), and $t_{\text{unocc–PC},i} = 12$ midnight. The impact of $T_{\text{occ–DL,max}}$ on peak load reduction is greater than that of other setpoint temperatures under demand-limiting. As $T_{\text{occ–DL,max}}$ increases, PLR decreases (greater peak load reduction). PLR also decreases as the demand-limiting start-time increases and its impact gets larger as $T_{\text{occ–DL,max}}$ increases.

It is interesting to compare the peak load reduction of demand-limiting strategies with that associated with increasing the occupied setpoint for night setup control. Fig. 13 shows the impact of $T_{\text{occ–NS}}$ on PLR$_{\text{NS}}$. As $T_{\text{occ–NS}}$ (setpoint temperature during occupied period under NS) increases, PLR$_{\text{NS}}$ decreases about 10% compared to the peak cooling
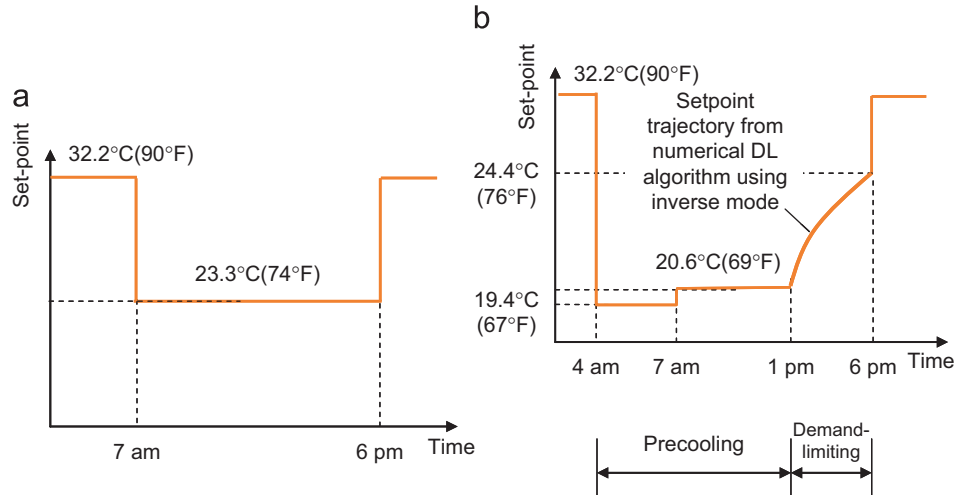
b

Fig. 14. Setpoint schedules for testing: (a) night-setup control and (b) model-based demand-limiting strategy.

load under NS with an occupied setpoint temperature of 23.3 °C (74 °F). The effect on peak load reduction of raising this setpoint is significantly less than the effect of employing the demand-limiting control strategy.

6. Experimental evaluation of demand-limiting control

6.1. Test procedures

In order to validate the level of demand reduction predicted with the inverse model for demand-limiting control, testing was conducted over 14 days from August 14 to 27. The setup of the tests was identical to the setup used by Braun et al. [14] with the same internal gains, clear windows having no blinds, and with no additional internal mass. The testing began on August 14 with a conventional night setup strategy in order to establish a good baseline. The strategy was switched to the model-based demand-limiting strategy for the period from August 20 and to 27. Unfortunately, the weather was very mild and overcast for most of the test period.

Fig. 14 describes the setpoint schedules for the night setup and model-based demand-limiting strategies implemented during testing. The occupied period was from 7 AM to 6 PM, whereas the period for demand-limiting was 1 to 6 PM. With an afternoon demand-limiting period, results from the previous section indicate that a precool start time of 4 am is near optimal. Precooling occurred at 19.4 °C (67 °F) from 4 AM to 7 AM followed by a period of operation with a setpoint 20.6 °C (69 °F) until 1 PM. During the demand-limiting tests, the setpoint was raised from 20.6 °C (69 °F) to 24.4 °C (76 °F) between 1 and 6 PM using a trajectory obtained from an inverse model. The model used forecasts of weather conditions and estimated setpoints that would minimize the peak cooling requirement during the demand-limiting period. The setpoints were entered into the main control system manually at 10-min intervals.

Simple weather prediction models were used to obtain short-term forecasts of ambient temperature and global solar radiation for the demand-limiting period and are expressed as

$$T_{a,k}^* = \frac{1}{N_{avg}} \left(\sum_{n=1}^{N_{avg}} T_{a,k-24*n} \right) + (T_{a,12} - T_{a,12}^*),$$

for $k = 13, \ldots, 24,$ (16)

$$G_{sol,k}^* = \frac{1}{N_{avg}} \left(\sum_{n=1}^{N_{avg}} G_{sol,k-24n} \right) \left(\frac{G_{sol,12}}{G_{sol,12}^*} \right),$$

for $k = 13, \ldots, 24,$ (17)

where $T_{a,k}^* =$ predicted ambient temperature at time k, $T_{a,k} =$ actual measured ambient temperature at time k, $N_{avg} =$ number of days used for averaging, $G_{sol,k}^* =$ predicted global horizontal solar radiation at time k, and $G_{sol,k} =$ actual measured global horizontal solar radiation at time k.

The weather predictions were performed within the hour before 1 PM and then used throughout the demand-limiting period to estimate the setpoint variation that would minimize the peak cooling demand. Zone temperatures for the general spaces were controlled at the same setpoints as for the test rooms. Integrated RMS (root-mean-squared) errors of weather prediction for the period of 1 to 6 PM during testing were 1.69 °C (3.04 °F) and 216.9 W/m² (68.75 Btu/h ft²), respectively. The maximum global horizontal solar radiation during the period was 896.3 W/m² (284.13 Btu/h ft²). The ambient temperature prediction model worked well but had difficulty predicting sudden changes due to weather fronts. Global solar radiation was predicted quite well on clear days but not on partly cloudy days having rapid changes. Much better accuracy would be possible if the weather predictions were updated continuously, as would occur for an on-line application.

Table 7
Comparison of weather conditions for selected phase 1 test days

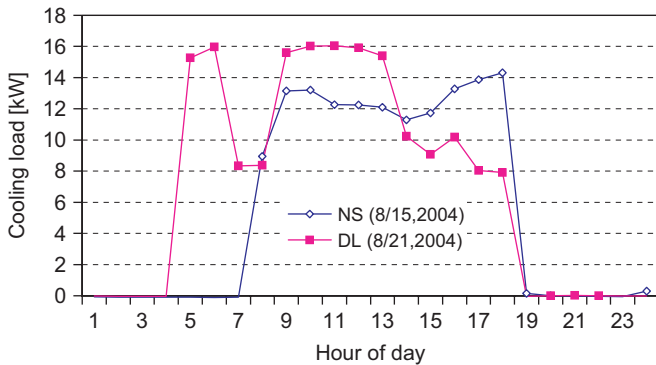| Date	Ambient temperature [°C (°F)]				Global horizontal solar radiation [W/m^2 (Btu/h-h-ft^2)]			
	Max	Min	RMSD	RMSD (%)	Max	Min	RMSD	RMSD (%)
August 15, 2004	24.01 (75.21)	11.0 (51.80)	–	–	873.8 (276.99)	10.00 (3.17)	–	–
August 21, 2004	23.99 (75.18)	11.92 (53.45)	1.62 (2.91)	3.87	801.2 (253.98)	10.03 (3.18)	38.08 (12.07)	4.36

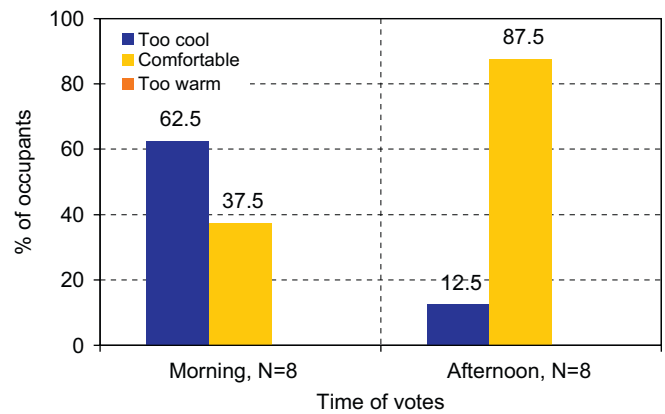Fig. 15. Comparison of cooling loads for two selected comparable days.

Fig. 16. Comfort evaluation for demand-limiting testing.

6.2. Peak demand reduction and comfort results

For most days during testing, the sky was cloudy and the peak ambient temperature was below 32.2 °C (90 °F). There were a few moderate test days having clear and similar ambient temperature conditions that allow comparison of demand-limiting and night setup control strategies. Table 7 shows comparison of ambient conditions for two selected days, August 15 and 21, which are thought to be closest among the test days for the night setup and demand-limiting strategies. Minimum, maximum, and integrated root-mean-squared differences (RMSD) in hourly values for ambient temperature and solar radiations between the two comparable days are shown. The ambient temperatures on August 21 were a little lower than those for August 15 during the morning and early afternoon. In addition, the solar was a little lower throughout the day.

Fig. 15 compares combined cooling loads for the eight test zones operated under the model-based demand-limiting strategy with that under night setup control for the selected days. Under night setup control, the peak cooling load occurs late in the day due to solar gains through west facing windows. The peak for the demand-limiting strategy occurs during the morning hours when the facility is operated at a low setpoint temperature. During the demand-limiting period (1 to 6 PM), the peak cooling load was reduced by about 30% compared to night setup control. However, additional demand reduction would have been possible if the setpoint trajectory had produced a flatter cooling load profile. The actual load profile was not flat due to imperfect building modeling and weather predictions. The model could be improved with more data for training. The weather predictions could be improved if

the forecasts were updated every hour during application of the strategy. Even so, the demand reduction results were very significant on this relatively cool day.

Fig. 16 shows comfort survey results for morning and afternoon periods on days where demand-limiting was employed during testing. The variable N denotes the number of participants in the comfort survey for each time period. Because of a small number of participants, the comfort results from the survey were compressed into three categories: too cool (combines cold and cool), comfortable (combines slightly cool, neutral, and slightly warm) and too warm (combines warm and hot). A slight majority of the occupants felt uncomfortably 'too cool' in the morning. This was probably due to precooling that occurred at 19.4 °C (67 °F) during the early morning from 4 to 7 AM. In the afternoon, most of the occupants were comfortable. Fortunately, the impact of morning precooling temperature on demand reduction is relatively small as demonstrated in the previous section. As a result, there is an opportunity to raise this temperature to improve comfort conditions. Lee and Braun [12] found a relatively small impact on occupant comfort for this facility with strategies that precooled at 21.1 °C (70 °F) and performed demand limiting between 21.1 °C (70 °F) and 25.5 °C (78 °F).

7. Conclusions

A demand-limiting control methodology was developed that uses an inverse building model trained with field measurements. The methodology was applied to a building representative of small commercial applications. The inverse

Table A.1
Estimated parameters of inverse model for ERS building

Parameter	Value	Parameter	Value
$C_{e,1}$ (kJ/K)	45357.35 (23883.59 Btu/°F)	$R_{e,1}$ (K/W)	0.0007545 (0.000398 °F h/Btu)
$C_{e,2}$ (kJ/K)	5421.59 (2854.82 Btu/°F)	$R_{e,2}$ (K/W)	0.008206 (0.004329 °F h/Btu)
$C_{i,1}$ (kJ/K)	3096.83 (1630.68 Btu/°F)	$R_{e,3}$ (K/W)	0.01602 (0.008449 °F h/Btu)
$C_{i,2}$ (kJ/K)	11402.98 (6004.41 Btu/°F)	$R_{i,1}$ (K/W)	0.00003412 (0.000018 °F h/Btu)
$C_{r,1}$ (kJ/K)	218293.19 (114945.54 Btu/°F)	$R_{i,2}$ (K/W)	140 (73.85 °F h/Btu)
$C_{r,2}$ (kJ/K)	948653.92 (499527.89 Btu/°F)	$R_{i,3}$ (K/W)	0.001331 (0.000702 °F h/Btu)
$C_{f,1}$ (kJ/K)	27936.52 (14710.39 Btu/°F)	$R_{r,1}$ (K/W)	0.00007772 (0.000041 °F h/Btu)
$C_{f,2}$ (kJ/K)	1188.67 (625.91 Btu/°F)	$R_{r,2}$ (K/W)	0.0003431 (0.000181 °F h/Btu)
$C_{z,eff}$ (kJ/K)	11382.22 (5993.48 Btu/°F)	$R_{r,3}$ (K/W)	0.006201 (0.003271 °F h/Btu)
τ_{eff}	0.697	$R_{f,1}$ (K/W)	0.003945 (0.002081 °F h/Btu)
Rwin (K/W)	0.006587 (0.003475 °F h/Btu)	$R_{f,2}$ (K/W)	0.002237 (0.001180 °F h/Btu)
		$R_{f,3}$ (K/W)	0.002775 (0.001464 °F h/Btu)

The total thermal capacitance for the ERS building was calculated as the sum of all the node capacitance values and found to be 197.3 MJ/K (103869 Btu/°F).

model was able to predict cooling loads within about 5% when trained with 14 days of data from Braun et al. [14] where precooling and night setup control strategies were applied to this facility. More importantly, the model very accurately predicted load shifting and peak load reduction for the load-shifting strategy tested by Braun et al. [14]. The trained model was then used in combination with the demand-limiting scheme to investigate the impact of different control strategy parameters on peak demand reduction. For afternoon demand-limiting periods, peak load reduction is relatively insensitive to the temperature and start time for precooling during the unoccupied period. In this case, most of the potential for demand reduction is realized when the zone temperature is maintained at the lower end of the comfort range for morning occupied hours and then adjusted upwards during the demand-limiting period to the high end of the comfort range following a trajectory that produces a constant cooling load. Predicted peak load reduction was about 30% for a demand-limiting period between 1 and 6 PM with zone temperatures maintained within the range of comfort. Unoccupied period precooling becomes important when demand-limiting is initiated during morning hours.

The model-based, demand-limiting strategy was implemented at the site resulting in a 30% reduction in peak cooling load when compared to conventional control for a 5-h afternoon demand-limiting period. These results are consistent with the simulation results.

Small commercial buildings are good candidates for utilization of thermal storage in building mass to reduce peak demands. However, even greater potential is possible for large commercial buildings because of a smaller ratio of external area to thermal mass, and the use of heavier weight materials.

Appendix A

Table A.1 gives building parameters that were estimated for the ERS building through training using data from both the Phase 1 and Phase 2 test periods.

References

[1] Catani MJ, Goodwin SE. Heavy building envelopes and dynamic thermal response. Journal of the American Concrete Institute 1976;73(2).

[2] Braun JE. Reducing energy costs and peak electrical demand through optimal control of building thermal storage. ASHRAE Transactions 1990;96(2):839–48.

[3] Ruud MD, Mitchell JW, Klein SA. Use of building thermal mass to offset cooling loads. ASHRAE Transactions 1990;96(2):820–9.

[4] Rabl A, Norford LK. Peak load reduction by preconditioning buildings at night. International Journal of Energy Research 1991; 15:781–98.

[5] Reddy TA, Norford LK, Kemption W. Shaving residential air-conditioning peaks by intelligent use of the building thermal mass. Energy 1991;16(7):1001–10.

[6] Keeney KR, Braun JE. A simplified method for determining optimal cooling control strategies for thermal storage in building mass. International Journal of HVAC&R Research 1996;2(1):59–78.

[7] Keeney KR, Braun JE. Application of building precooling to reduce peak cooling requirements. ASHRAE Transactions 1997;103(1): 463–9.

[8] Braun JE, Montgomery KW, Chaturvedi N. Evaluating the performance of building thermal mass control strategies. International Journal of HVAC&R Research 2001;7(4):403–28.

[9] Xu P, Haves P, Braun JE, Hope LT. Peak demand reduction from pre-cooling with zone temperature reset in an office building. In: Proceedings of the ACEEE 2004 summer study on energy efficient in buildings, 2004.

[10] Xu P, Haves P, Zagreus L, Piette M. Demand shifting with thermal mass in large commercial buildings (field tests, simulation and results). Lawrence Berkeley National Laboratory, CEC-500-2006-009; 2006.

[11] Chaturvedi N, Braun JE. An inverse grey-box model for transient building load prediction. International Journal of HVAC&R Research 2002;8(1):73–100.

[12] Lee K-H, Braun JE. An experimental evaluation of demand-limiting using building thermal mass in a small commercial building. ASHRAE Transactions 2006;112:1.

[13] Price BA, Smith TF. Description of the Iowa Energy Center Energy Resource Station: facility update III. Technical Report ME-TFS-00-001, The University of Iowa; 2000.

[14] Braun JE, Lawrence TM, Klaassen CJ, House JM. Demonstration of load shifting and peak load reduction with control of building thermal mass. In: Proceeding of the 2002 ACEEE conference on energy efficiency in buildings, Monterey, CA, USA, 2002.

[15] Thomas HR, Rees SW. The thermal performance of ground floor slabs—a full scale in situ experiment. Building and Environment 1999;34:139–64.

[16] Zhou Z, Rees SW, Thomas HR. A numerical and experimental investigation of ground heat transfer including edge insulation effects. Building and Environment 2002;37:67–78.

[17] Seem JE, Klein SA, Beckman WA, Mitchell JW. Transfer functions for efficient calculations of multi dimensional heat transfer. Journal of Heat Transfer—Transactions of the ASME 1989;111(1): 5–12.